Pretargeting with Cucurbituril–Adamantane Host–Guest Pair in Xenograft Models

Vilma I.J. Jallinoja[1,2], Courtney H. Abbriano[1], Kavita Bhatt[1], Amritjyot Kaur[1], David J. Schlyer[1,3], Paul J. Yazaki[4], Brandon D. Carney[1], and Jacob L. Houghton[1]

[1]Department of Radiology, Stony Brook University, Stony Brook, New York; [2]Chemical and Physical Biology Graduate Program, Vanderbilt University, Nashville, Tennessee; [3]Collider-Accelerator Department, Brookhaven National Laboratory, Upton, New York; and [4]Department of Immunology and Theranostics, Beckman Research Institute, City of Hope, Duarte, California

The goal of reducing the total-body radiation dose of macromolecule-based nuclear medicine with a 2-step pretargeting strategy has been achieved with several pretargeting methodologies in preclinical and clinical settings. However, the lack of modularity, biocompatibility, and in vivo stability in existing pretargeting agents obstructs their respective platforms' wide clinical use. We hypothesized that host–guest chemistry would provide an optimal pretargeting methodology. A cucurbit[7]uril host and an adamantane guest molecule form a high-affinity host–guest complex (association constant, $\sim 10^{14}$ M^{-1}), and in this work, we explored the use of this noncovalent interaction as the basis for antibody-based pretargeted PET. Along with the straightforward modularity of these agents, cucurbit[7]uril and adamantane are recognized to have high in vivo stability and suitability for human use, which is why we proposed this methodology as the ideal approach for pretargeted nuclear medicine. **Methods:** Three ^{64}Cu-labeled adamantane guest radioligands were developed, and their in vitro stability, lipophilicity, and in vivo blood half-lives were compared. The adamantane radioligands were analyzed for pretargeting using a cucurbit[7]uril-modified carcinoembryonic antigen–targeting full-length antibody, hT84.66-M5A, as the macromolecule pretargeting agent with 2 different dosing schedules. These molecules were evaluated for pretargeting in human pancreatic cancer BxPC3 and MIAPaCa-2 mouse xenografts using PET and in vivo biodistribution studies. The dosimetry of the cucurbit[7]uril–adamantane (CB7-Adma) pretargeting approach in men was calculated and compared with that of the directly ^{89}Zr-labeled hT84.66-M5A. **Results:** The adamantane radioligands possessed high in vitro stability up to 24 h (>90%). Pretargeted PET with CB7-Adma methodology resulted in specific tumor uptake ($P < 0.05$) with low background signal. The in vivo formed CB7-Adma complex was demonstrated to be stable, with high tumor uptake up to 24 h after radioligand injection (12.0 ± 0.9 percentage injected dose/g). The total-body radiation dose of the pretargeting strategy was only 3.3% that of the directly ^{89}Zr-labeled hT84.66-M5A. **Conclusion:** The CB7-Adma strategy is highly suitable for pretargeted PET. The exceptional stability of the pretargeting agents and the specific and high tumor uptake of the pretargeted adamantane radioligands provide great potential for the platform.

Key Words: pretargeting; host–guest chemistry; carcinoembryonic antigen; PET; adamantane

Pretargeted PET provides a quantitative, noninvasive whole-body in vivo profile of macromolecules with an overall lower total-body radiation dose than directly radiolabeled macromolecules (1,2). Pretargeting is a 2-step strategy involving administration of a target-binding macromolecule that accumulates at the target site over several days while the unbound macromolecule excretes from nontarget tissue. In a second step, a bioorthogonal small-molecule radioligand is administered (Fig. 1). The low molecular weight of the radioligand allows its target accumulation and excretion to occur more quickly than for the initial macromolecule. The work reported here harnesses host–guest complex formation as the specific pretargeting interaction between the macromolecule and the radioligand. We hypothesized that because of the high in vivo stability, modularity and low immunogenicity, the chosen host–guest pair, cucurbit[7]uril–adamantane (CB7-Adma; association constant, $\sim 10^{14}$ M^{-1}), makes an ideal interaction pair for pretargeted PET (3–5). The strong complex between the 2 molecules forms when the Adma guest with an adjacent positively charged moiety binds to the carbonyl framed cavity of the macrocyclic CB7 host molecule via multiple van der Waals and ion-dipole interactions. So far, the medical imaging applications using host–guest chemistry have been limited to preformed host–guest complexes to increase the stability or sensitivity of imaging agents (6–8). In nuclear medicine, the high-affinity noncovalent binding between CB7 and Adma molecules has remained minimally explored (9).

The reported work lays the foundation for the host–guest chemistry of the CB7-Adma–driven pretargeting platform. Three ^{64}Cu-labeled Adma guest molecules were synthesized and characterized: [^{64}Cu]Cu-NOTA-Adma (**1**), [^{64}Cu]Cu-NOTA-polyethylene glycol (PEG)$_3$-Adma (**2**), and [^{64}Cu]Cu-NOTA-PEG$_7$-Adma (**3**) (Fig. 2A). The in vivo profile of the ligands for pretargeting was evaluated using a CB7-modified carcinoembryonic antigen (CEA) targeting humanized full-length antibody (CB7-M5A) as the secondary pretargeting agent. To study the potential of the platform, we investigated 2 pretargeting lag time schedules, 72 and 144 h. The pretargeting studies were performed on BxPC3 (CEA-positive) and MIAPaCa-2 (CEA-negative) human pancreatic cancer mouse xenografts (10–12).

The biodistribution and dosimetry of the pretargeted Adma radioligand were compared with those of a directly ^{89}Zr-labeled M5A. We hypothesized that the high stability, mutual high affinity, and human compatibility of the proposed CB7-Adma pretargeting agents would provide a great basis for a widely applicable pretargeting platform.
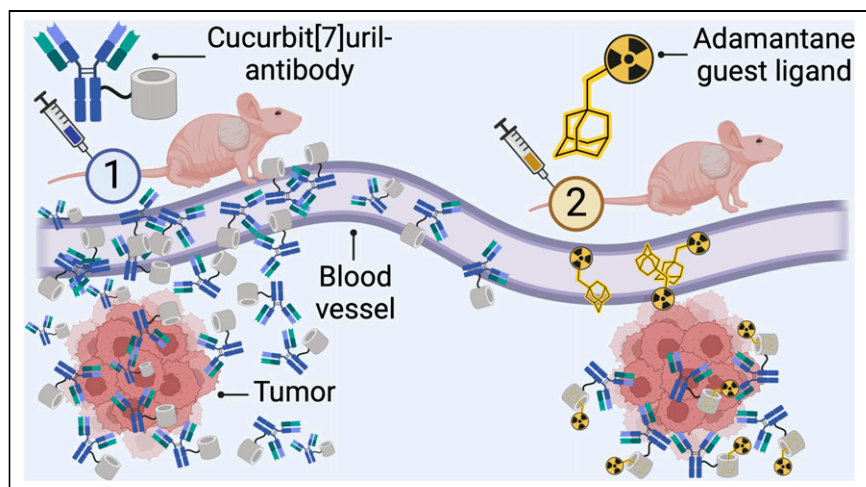
FIGURE 1. Illustration of 2-step CB7-Adma pretargeting approach.

MATERIALS AND METHODS

Development of Adma Radioligands

Detailed information on synthesis and characterization of the precursors for Adma radioligands **1**–**3** is provided in Supplemental Figures 1–3 (supplemental materials are available at http://jnm.snmjournals.org) To synthesize **1**–**3**, [^{64}Cu]CuCl$_2$ in 0.05 M HCl (1.5–7.4 μL; 47–260 MBq) was mixed with 0.2 M NH$_4$OAc (pH 5.5; 50–150 μL) in an Eppendorf tube. The respective precursors for **1, 2,** and **3** (1–5 μL in DMSO) were added to the solution, followed by incubation of the reaction at room temperature for 10 min. The reaction was monitored with radio–high-performance liquid chromatography using a method described in the supplemental materials. Because of the high radiolabeling yield, no purification was required.

Synthesis and Characterization of Modified M5A Molecules

CB7-M5A and deferoxamine-conjugated M5A (DFO-M5A) were prepared as previously described (*13,14*). The quality control of both modified antibodies was performed with size-exclusion chromatography, and the immunoreactivity was determined via cellular binding using the Lindmo assay (*15*) as previously reported (*14*). The number of CB7 moieties per monoclonal antibody (mAb) was determined as previously reported (*13*).

^{89}Zr Labeling of DFO-M5A

[^{89}Zr]Zr(C$_2$O$_4$)$_2$ in 0.1 M oxalic acid (86.2 MBq; 46 μL) was neutralized to pH 7.4 using 1 M NaHCO$_3$. DFO-M5A (900 μg; 6 nmol in 450 μL in phosphate-buffered saline [PBS], pH 7.4) was added to the solution of ^{89}Zr, and the labeling reaction was incubated at room temperature for 1 h. The labeling reaction yield was checked with radio–thin-layer chromatography using instant thin-layer chromatography silica gel glass microfiber chromatography paper and 50 mM ethylenediaminetetraacetic acid as the mobile phase. The synthesized [^{89}Zr]Zr-DFO-M5A was purified with a PD10 desalting column using PBS as the elution buffer. The radiochemical purity of the purified product was determined using the previously described radio–thin-layer chromatography method.

In Vitro Stability and Plasma Protein Binding of 1–3

The in vitro stability of **1**–**3** was studied in PBS and in bovine plasma at 37°C. First, freshly synthesized radioligand (**1**–**3**; 1.5 nmol; 3.0–3.9 MBq in 100 μL of 0.2 M NH$_4$OAc, pH 5.5) was added to an Eppendorf tube with PBS (1 mL). The samples were incubated at 37°C for 1, 6, or 24 h, after which they were analyzed with radio–high-performance liquid chromatography. To study the ligands' stability in plasma, freshly synthesized radioligands **1**–**3** (1.4 MBq in 5 μL of 0.2 M NH$_4$OAc, pH 5.5) were mixed with bovine plasma (100 μL). The samples were incubated at 37°C for 1, 6, or 24 h followed by an addition of cold acetonitrile (100 μL). The sample was centrifuged for 5 min (10,000 rpm). Supernatant was collected and centrifuged for a second time, after which it was diluted with H$_2$O (300 μL) and run on radio–high-performance liquid chromatography. The formed pellet was measured for radioactivity and compared with the initial total activity to determine the protein-bound fraction. Both stability assays were done in triplicate.

Distribution Coefficient (Log D) Measurement of Guest Radioligands

Freshly synthesized radioligands **1**–**3** (586–610 kBq; 13 μL in 0.2 M NH$_4$OAc, pH 5.5) were added to an Eppendorf tube containing PBS (600 μL) and 1-octanol (600 μL). The mixture was stirred on a ThermoMixer (Eppendorf) for 10 min (900 rpm) at room temperature and was then centrifuged for 5 min (1,000 relative central force); 200 μL of each phase were transferred, and the samples were weighed and counted on a γ-counter to determine the relative amount of radioactivity in each phase. The log D value was calculated as log$_{10}$ (% radioligand
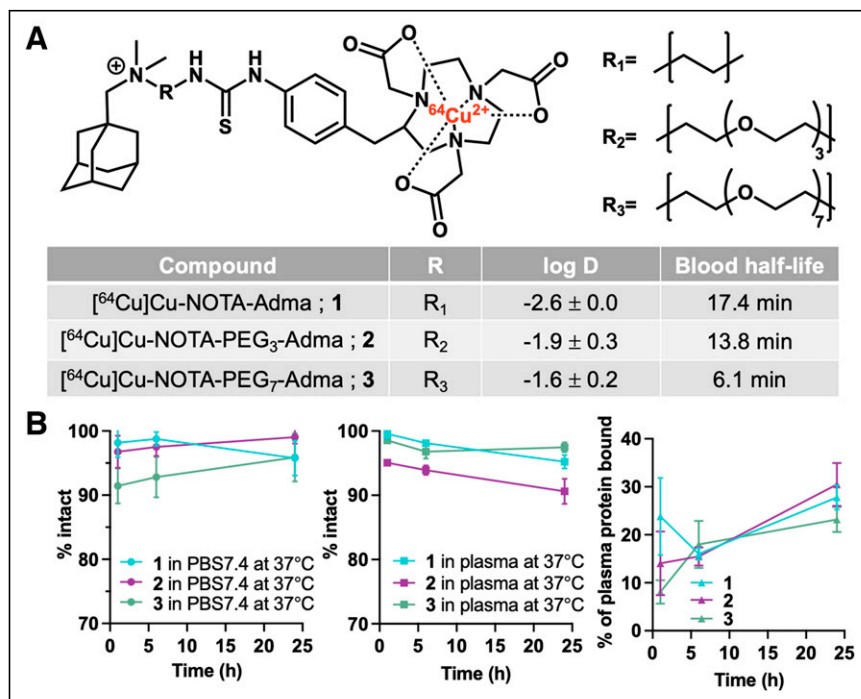

FIGURE 2. (A) Chemical structure of [^{64}Cu]Cu-NOTA-Adma (**1**), [^{64}Cu]Cu-NOTA-PEG$_3$-Adma (**2**), and [^{64}Cu]Cu-NOTA-PEG$_7$-Adma (**3**) and their respective log D and blood half-lives. (B) In vitro stability of **1**–**3** in PBS (pH 7.4) and in bovine plasma at 37°C and their plasma protein binding.

Compound	R	log D	Blood half-life
[^{64}Cu]Cu-NOTA-Adma ; **1**	R$_1$	-2.6 ± 0.0	17.4 min
[^{64}Cu]Cu-NOTA-PEG$_3$-Adma ; **2**	R$_2$	-1.9 ± 0.3	13.8 min
[^{64}Cu]Cu-NOTA-PEG$_7$-Adma ; **3**	R$_3$	-1.6 ± 0.2	6.1 min

in 1-octanol/% radioligand in PBS). The experiment was done in triplicate.

BxPC3 Cell Interaction with 2

Freshly synthesized **2** (354 kBq; 10 μL) or [^{64}Cu]CuCl$_2$ in 0.2 M NH$_4$OAc, pH 5.5 (407 kBq; 10 μL), was mixed with RPMI-1640 medium containing a 0.3 g/L concentration of glutamine, 25 mM 4-(2-hydroxyethyl)-1-piperazineethanesulfonic acid, 1% (v/v) penicillin–streptomycin, and 10% (v/v) fetal bovine serum (12 mL). Medium (1 mL) was measured into the wells of a 6-well plate that had been plated with 0.75×10^6 BxPC3 cells the day before. The cells were incubated with the medium for 2, 4, or 6 h at 37°C followed by treatment with 0.05 M glycine, pH 2.8. Finally, the cells were lysed by being incubated with 1.0 M NaOH. The medium, glycine, and NaOH solutions were collected and measured with a γ-counter to determine the unbound, membrane-bound, and internalized fraction of each radioactive agent.

1–3 in Healthy Mice

To determine the blood half-life of each Adma radioligand, freshly synthesized radioligands **1–3** (13.6–14.8 MBq; 1.5 nmol in 100 μL of PBS) were injected intravenously into healthy female nude mice ($n = 3$). Blood was drawn from the saphenous vein at 6 different time points after injection (2, 5, 15, 30, 60, and 120 min). The collected blood samples were weighed and measured with a γ-counter to determine the percentage injected dose per gram (%ID/g) for each sample. In addition to studying the blood half-life of each radioligand, we studied the renal excretion of **2** at early time points in healthy female nude mice by collecting urine at 20 and 60 min after radioligand injection. Further descriptions of both experiments are detailed in the supplemental materials.

Pretargeting with 1–3

Experimental cohorts of BxPC3 tumor–bearing female nude mice ($n = 4$–5/cohort) were injected intravenously with CB7-M5A (0.7 nmol; 100 μg in 150 μL in PBS) followed 72 h later with an intravenous injection of **1–3** (1.5 nmol; 10.2–13.9 MBq in 150 μL in PBS). For pretargeting with **2**, a 144-h lag time between the antibody and radioligand was also investigated. The cohorts were euthanized for in vivo biodistribution 4, 8, or 24 h after radioligand injection, and the 24-h cohort was also imaged with a small-animal PET/CT scanner (Siemens Inveon) at 4, 8, and 24 h after radioligand injection before euthanasia. An additional cohort per time point for pretargeted **2** was assigned, which was euthanized 2 h after radioligand injection for dosimetry calculations. The corresponding control cohort ($n = 4$/cohort) for each ligand was injected intravenously only with **1–3** and euthanized for in vivo biodistribution studies 24 h after injection.

[^{89}Zr]Zr-DFO-M5A In Vivo Profile in Tumor Models

A cohort of BxPC3 and MIAPaCa-2 tumor–bearing female nude mice ($n = 4$/cohort) was injected intravenously with [^{89}Zr]Zr-DFO-M5A (0.7 nmol; 100 μg; 2.3–3.4 MBq in 200 μL in PBS). The mice were imaged with a small-animal PET/CT scanner 72 h after injection, followed by in vivo biodistribution studies.

Pretargeting with 2 in MIAPaCa-2 Xenografts

A cohort of MIAPaCa-2 tumor–bearing female nude mice ($n = 4$) was injected with CB7-M5A (0.7 nmol; 100 μg in 150 μL in PBS) intravenously 72 h before an injection of **2** (1.5 nmol; 8.8–10.1 MBq in 150 μL in PBS). The mice were imaged with a small-animal PET/CT scanner 24 h after radioligand injection, followed by in vivo biodistribution studies.

The Dosimetry of Pretargeted 2

The estimated dosimetry of the pretargeted **2** in a man (70 kg) was calculated on the basis of the in vivo biodistribution of the pretargeted **2** in BxPC3 tumor–bearing mice. The biodistribution data were fitted

using a linear interpolation between time points. The linear function of each organ was used to interpolate the concentration at intervals of 1 h to better estimate the kinetics. The integration time was extended 48 h with the assumption that the %ID per organ was constant after the first 24 h and that the only change in concentration between 24 and 48 h was due to radioactive decay. A trapezoidal approximation was then used to obtain the integral over the time intervals. These residence times were used to estimate the absorbed dose to a human subject using the OLINDA program (*16*) with the adult human male model and no bladder clearance. The %ID to the large intestine was divided equally between the right and left colon for input into the OLINDA model for a man. The dose to the rest of the body was not used in this calculation.

Statistical Analysis

Statistical analysis for all data from the biodistribution and in vitro assays was performed with 2-tailed unpaired *t* tests using Prism (GraphPad Software, Inc.). A *P* value between 2 groups of less than 0.05 was considered significant. At least 4 mice were used for each pretargeting cohort. All in vitro experiments were performed in triplicate unless otherwise noted.

RESULTS

Development of Pretargeting Agents

Each of the 3 radioligands was synthesized and radiolabeled efficiently and in good yields. Precursors for **1, 2,** and **3** were synthesized with overall yields of 14.5%, 36.2%, and 14.1%, respectively, and with respective chemical purities of 97.6%, 97.2%, and 95.8% (Supplemental Figs. 4–6). Radioligands **1–3** were produced by radiolabeling their corresponding precursors with high radiochemical yields of 97.6% ± 1.5%, 98.5% ± 0.7%, and 96.7% ± 0.0%, respectively, and with purity of 97.5% ± 1.0%, 98.3% ± 1.8%, and 98.9% ± 0.7%, respectively ($n = 3$) (Supplemental Figs. 7–9).

CB7 conjugated antibody was synthesized with an overall recovery yield of 83%. Each M5A was determined to have 0.8 ± 0.0 CB7 ($n = 3$) moieties on average. Quality control testing of the CB7-M5A indicated that no aggregation or fragments were present (Supplemental Fig. 10). The immunoreactivity of the CB7-conjugated antibody was 95.7% ± 0.7% ($n = 3$).

In Vitro Characterization of 1–3

To compare the 3 radioligands, we performed in vitro analysis on each to determine their relative pharmacologic characteristics and suitability for in vivo pretargeting experiments. **1–3** demonstrated great in vitro stability in PBS and in bovine plasma (Fig. 1B; Supplemental Tables 1 and 2). At 24 h, 95.8% ± 2.2%, 99.0% ± 0.8%, and 95.9% ± 3.1% of **1, 2,** and **3**, respectively, was still intact in PBS and 95.2% ± 0.9%, 90.6% ± 1.6%, and 97.5% ± 0.6%, respectively, remained intact in bovine plasma samples. No free ^{64}Cu was observed in any of the stability samples, suggesting that the radioligands were sufficiently stable for the application. At the 1-h time point, the Adma radioligands exhibited decreased plasma binding as the length of polyethylene glycol (PEG) linker increased (23.8 ± 6.6 [**1**], 14.0 ± 5.4 [**2**], and 8.1 ± 2.0 [**3**]). Additionally, the fraction of protein-bound radioligand grew over time to the last time point of 24 h (27.8 ± 2.1 [**1**], 30.5 ± 3.7 [**2**], and 23.2 ± 2.1 [**3**]). These differences among the molecules were not significant ($P > 0.05$).

On the basis of the cell internalization assay in BxPC3 cells, **2** did not bind to the cell membrane (0.1% ± 0.1%) or get internalized (0.0% ± 0.0%) even after a 6-h incubation period (Supplemental Fig. 11). [^{64}Cu]CuCl$_2$ demonstrated significantly higher internalization (5.2% ± 0.3%; $P = 0.002$) than **2,** confirming that

the ^{64}Cu-NOTA complex of **2** remained intact for the duration of the experiment.

Development of DFO-Modified Antibody

Quality control testing indicated that the DFO-conjugated M5A antibody was intact, and no fragments or aggregates were detected (Supplemental Fig. 10). The overall recovery yield was 85%. The immunoreactive fraction of DFO-M5A was 89.6% ± 2.1%, which was suitable for in vivo analysis.

1–3 in Healthy Mice

To determine the route and relative rate of clearance of the radioligands, we investigated their blood half-life. Additionally, because we expected a combination of both renal and hepatobiliary clearance, we collected urine at time points earlier than the first biodistribution time point. The in vivo blood half-life experiments revealed that the blood half-life correlated negatively with the number of PEG units incorporated in the radioligand (Fig. 2A; Supplemental Fig. 12). The ligands' blood half-lives decreased as the PEG-linker length increased (**1,** 17.4 min; **2,** 13.8 min; **3,** 6.1 min). Urine samples at 20 and 60 min after injection of **2** into healthy mice indicated that the radioligand demonstrated high renal clearance at these early time points (680 ± 210 and 1,050 ± 450 %ID/g, respectively) (Supplemental Table 3).

In Vivo Biodistribution of Pretargeted 1–3

In vivo biodistribution studies were performed to assess the relative effectiveness of the 3 radioligands for pretargeting of tumors in a mouse model. Of the 3 Adma radioligands that were studied with a 72-h lag time schedule, only pretargeted **1** and **2** demonstrated significantly higher tumor uptake than their respective control cohorts (**1,** $P = 0.005$; **2,** $P = 0.003$; Supplemental Tables 4 and 5). Pretargeted **3** resulted in almost 4 times higher average tumor uptake than control (3.9 ± 2.1 %ID/g and 0.0 ± 0.0 %ID/g, respectively; Supplemental Table 6). However, differences in tumor uptake between the cohorts were not significant ($P = 0.053$). Tumor uptake increased over time in all cohorts, yet the highest average tumor uptake was with pretargeted **2** (**1,** 8.9 ± 2.0 %ID/g; **2,** 12.0 ± 0.9 %ID/g; **3,** 3.9 ± 2.1 %ID/g) (Fig. 3). To demonstrate that our pretargeting platform may be suitable for clinical applications without the use of clearing agents, we also explored the best-performing radioligand (**2**) with a 144-h lag time, which is more aligned with the biologic half-life of mAbs in humans. For the pretargeted **2,** tumor uptake was lower when administration was at 144 h than at 72 h after CB7-M5A injection (144 h: 5.3 ± 1.4 %ID/g; $P = 0.01$), but the tumor-to-blood uptake ratio was substantially higher for the 144-h cohorts (Supplemental Tables 7 and 8).

The presence of all Adma radioligands in the blood pool was significantly higher in the pretargeting cohorts than in their corresponding control cohorts ($P = 0.001$, $P = 0.0006$, and $P = 0.01$ for **1, 2,** and **3,** respectively, with a 72-h lag time), revealing that the Adma radioligands bound to the remaining CB7-M5A circulating in the blood. However, when the lag time was extended from 72 to 144 h, the presence of the pretargeted **2** in the blood was not significantly higher than in control studies when only **2** was administered ($P = 0.13$), suggesting that less of **2** was binding to the CB7-M5A in the blood with the longer lag time (Supplemental Table 7). The lower presence of **2**-bound CB7-M5A circulating in the blood pool likely contributed to the fact that tumor uptake of pretargeted **2** was lower at later time points with the extended lag time. Initially at the 4-h time point, tumor uptake of pretargeted **2** was similar with 72- and 144-h lag times (3.5 ± 1.1 %ID/g and 3.2 ± 1.4 %ID/g, respectively).

All 3 pretargeted radioligands were excreted through the kidneys/bladder and gastrointestinal tract. With a 72-h lag time, excretion was the slowest for pretargeted **3.** For pretargeted **2,** excretion through the intestine was suggested to be slower with a longer lag time of 144 h. However, the SDs of the %ID/g values were large for the organ since feces were not removed from the large-intestine samples, a fact that could partly explain the difference between the lag time cohorts. By 24 h after injection, the excretion was complete for **1–3.** Despite the low kidney retention at 4 h with pretargeted **1–3** (<1.0 %ID/g; Supplemental Tables 4 and 7), **2** demonstrated early renal clearance in healthy mice (Supplemental Table 3).

As expected, tumor-to-blood ratios increased over time with the pretargeted ligands (Supplemental Table 8). The difference between the first and last time points was significant only with pretargeted **2** with a 72-h lag time (4 h, 2.3 ± 1.5; 24 h, 5.8 ± 0.4 [$P = 0.008$]). The low presence of **2** in the blood pool with the 144-h lag time resulted in a higher tumor-to-blood ratio at 24 h (16.7 ± 4.6) than under any other studied conditions.

As was expected from the CEA expression differences in BxPC3 and MIAPaCa-2 cells (Supplemental Fig. 13), tumor uptake of the pretargeted **2** was significantly lower in MIAPaCa-2 tumor models than in BxPC3 (0.5 ± 0.1 vs. 12.0 ± 0.9 %ID/g, respectively; $P = 0.003$), demonstrating the specificity of interaction of the radioligands with the tumors (Fig. 4D).

Pretargeted PET 1–3

PET imaging of the pretargeted radioligands **1–3** in BxPC3 tumor–bearing nude mice successfully delineated the tumor mass at all time points (Fig. 5; Supplemental Fig. 14). The images confirmed the in vivo biodistribution data, showing that the tumor uptake and tumor-to-background signal increased over time up to the last time point. Tumor uptake of the pretargeted radioligands **1–3** varied, at 3.8–17.1, 14.5–24.0, and
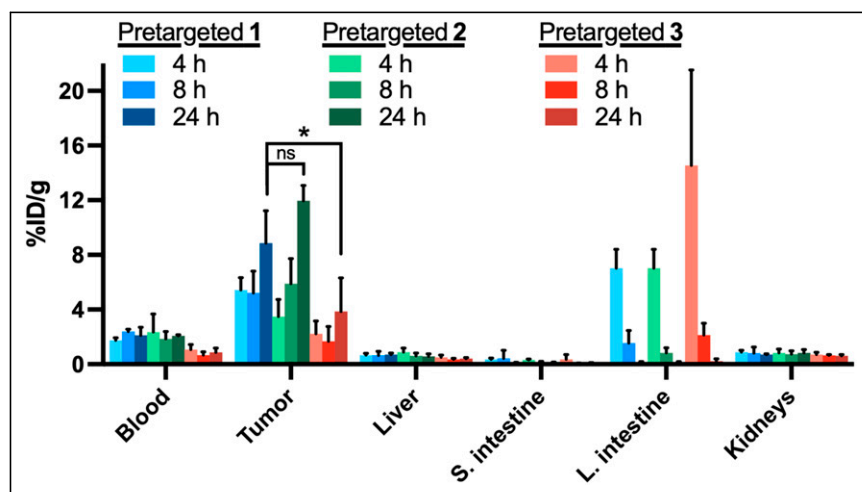

FIGURE 3. In vivo biodistribution of pretargeted [^{64}Cu]Cu-NOTA-Adma (**1**), [^{64}Cu]Cu-NOTA-PEG$_3$-Adma (**2**), and [^{64}Cu]Cu-NOTA-PEG$_7$-Adma (**3**) in BxPC3 tumor–bearing nude mice. *$P < 0.05$. ns = not significant.
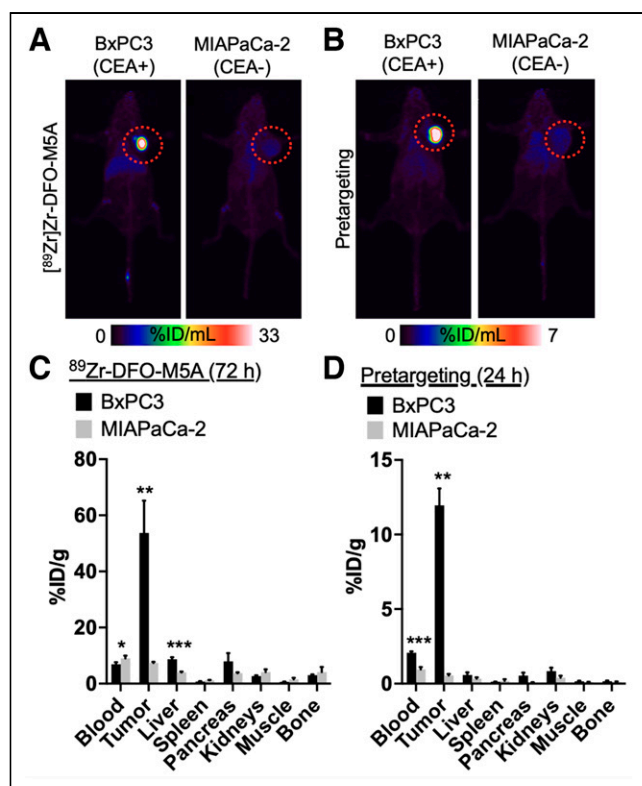
FIGURE 4. In vivo profile of [^{89}Zr]Zr-DFO-M5A at 72 h after injection and pretargeted **2** at 24 h after injection in BxPC3 and MIAPaCa-2 tumor–bearing female nude mice. Maximum-intensity-projection PET images of [^{89}Zr]Zr-DFO-M5A (A) and pretargeted **2** (B), and in vivo biodistribution of [^{89}Zr]Zr-DFO-M5A (C) and pretargeted **2** (D). Mice administered **2** were injected with CB7-M5A 72 h beforehand. Location of tumor on right shoulder is encircled.

2.8–13.1 %ID/mL, respectively, with the 72-h lag time and 3.8–7.9 %ID/mL with the 144-h lag time at 24 h after radioligand injection. For the pretargeted **2** in MIAPaCa-2 tumor–bearing mice, the tumor uptake values were between 0.8 and 1.4 %ID/mL, indicating that there was no specific uptake in the tumors due to the lack of CEA expression (Fig. 4B).

In Vivo Profile of [^{89}Zr]Zr-DFO-M5A in Xenograft Models

To compare uptake in antigen-expressing and antigen-negative cell lines with M5A, we used directly labeled [^{89}Zr]Zr-DFO-M5A. The in vivo profile of [^{89}Zr]Zr-DFO-M5A in the subcutaneous tumor mouse models of BxPC3 and MIAPaCa-2 revealed varying tumor uptake between the models. The findings aligned with the Western blotting results on the CEA expression of the cell lines, as well as with previously published results from the same cell lines (Supplemental Fig. 13) (10–12). The CEA-positive BxPC3 xenografts demonstrated higher tumor uptake than the CEA-negative xenografts of MIAPaCa-2 (53.7 ± 10.0 vs. 7.3 ± 0.3 %ID/g, respectively; P = 0.004) (Fig. 4C). On the basis of these imaging experiments, the tumor-to-background signal was higher in the BxPC3 cohort than in MIAPaCa-2, and the tumor uptake values in both tumor models supported the findings of the in vivo biodistribution studies (BxPC3, 50.4 ± 8.9 %ID/mL; MIAPaCa-2, 4.8 ± 0.2 %ID/g) (Fig. 4A).

Dosimetry of Pretargeted 2

To determine the dosimetric advantages of our pretargeting method, we calculated the dosimetry for our approach and compared it with that of the directly labeled [^{89}Zr]Zr-DFO-M5A. The estimated
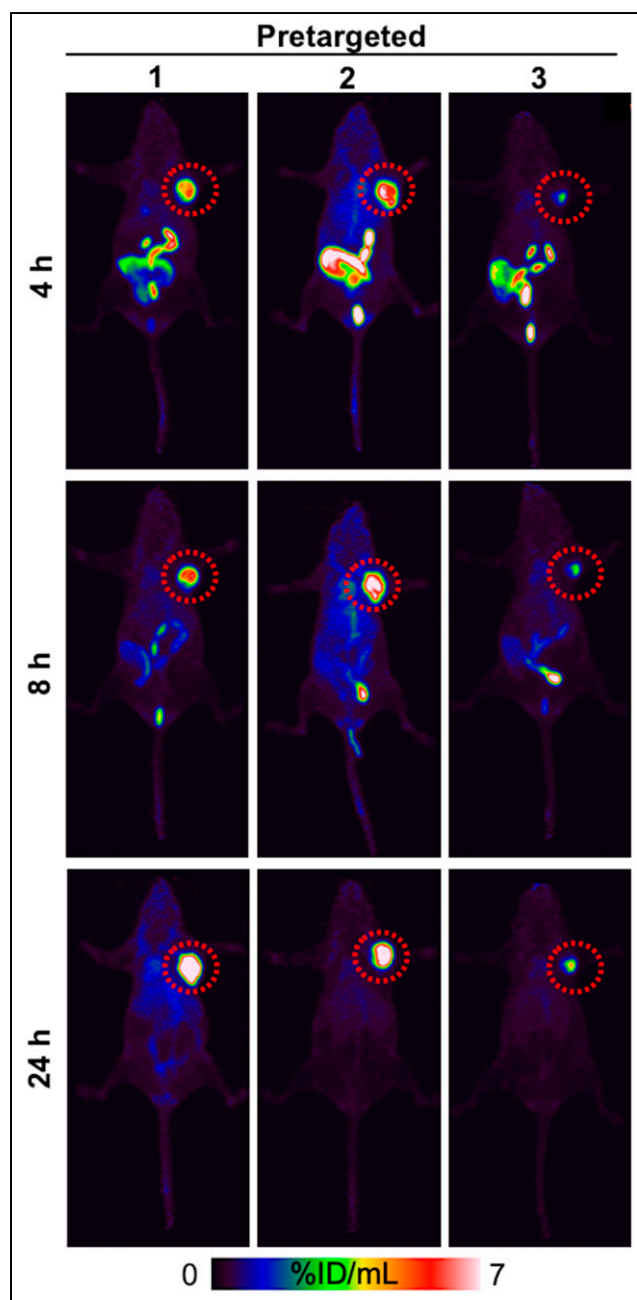

FIGURE 5. Maximum-intensity-projection PET images of pretargeted [^{64}Cu]Cu-NOTA-Adma (**1**), [^{64}Cu]Cu-NOTA-PEG$_3$-Adma (**2**), and [^{64}Cu]Cu-NOTA-PEG$_7$-Adma (**3**) in BxPC3 tumor–bearing nude mice at 4, 8, and 24 h after radioligand injection with 72-h lag time in pretargeting schedule. Location of tumor on right shoulder is encircled.

dose of a man for pretargeted **2** demonstrated that the CB7-Adma pretargeting approach resulted in much lower organ doses than did use of [^{89}Zr]Zr-DFO-M5A, whose dosimetry analysis was reported earlier by our laboratory (Supplemental Table 9) (14). In all investigated organs, the dose of pretargeted **2** was reduced severalfold compared with the directly radiolabeled M5A. The dose-limiting organ for use of directly radiolabeled antibodies is often red marrow, and here its dose with [^{89}Zr]Zr-DFO-M5A was found to be almost 70-fold higher than that of the pretargeted **2**. The reported injected clinical doses of ^{89}Zr-labeled mAbs vary between 37 and

185 MBq (*17,18*). In this regard, with an estimated 110-MBq clinical dose of [^{89}Zr]Zr-DFO-M5A, the effective dose would be 95.5 mSv. A clinical dose of 150 MBq of pretargeted **2**, however, would give rise to a lower effective dose of 6.0 mSv while still providing the necessary tumor–to–nontarget tissue uptake ratios to clearly delineate CEA-expressing tumors.

DISCUSSION

We have demonstrated in this work that host–guest CB7-Adma pretargeted PET shows specific and exceptionally high tumor uptake and tumor-to-background signal (Fig. 3; Supplemental Tables 4–8). The efficacy of the pretargeting methodology was evaluated with 3 ^{64}Cu-labeled Adma radioligands. The pretargeted radioligand with the best in vivo profile, **2**, was also studied with an additional lag time. Since the motivation for the studies was development of a pretargeting platform, the dosimetry of a directly radiolabeled [^{89}Zr]Zr-DFO-M5A and CB7-M5A pretargeted **2** was compared (Supplemental Table 9). Although the isotopes were not matched for these experiments, [^{89}Zr]Zr-DFO-M5A was chosen because ^{89}Zr is the most clinically relevant isotope for PET imaging with mAbs and provides information on the biologic fate of the mAbs at 5–7 d after injection, whereas ^{64}Cu-based PET with mAbs is useful for only about 2 d after injection, when there is still very low tumor–to–nontarget tissue uptake, especially in the blood.

The difference among **1, 2,** and **3** was observed in their respective blood half-lives and log D values, which resulted in the ligands' having variance in their tumor uptake and clearance profile. The number of PEG units incorporated in the Adma radioligand correlated negatively with the compound's log D value and blood half-life. The same correlation between the number of PEG units and the log D value was observed earlier by our laboratory with ferrocene radioligands designed for pretargeting (*14*). As has been reported earlier, with a higher number of hydrophilic PEG units the expectation is to have lower respective log D values (*19*). In addition to exploring the use of other linkers, our laboratory is investigating why the opposite trend was observed with **1**–**3**.

In turn, the log D values of **1**–**3** negatively correlated with the blood half-lives. This trend toward diffusion of more hydrophilic compounds from the bloodstream through the cell membrane at a lower rate, resulting in a longer blood half-life, has been established before (*20,21*). The difference in tumor uptake of pretargeted **1** and **2** was not significant, despite their relative difference in blood half-life. However, the Adma radioligand with the shortest blood half-life, **3,** resulted in the lowest tumor uptake, which was determined to be significant compared with pretargeted **1** and **2**. This positive correlation between blood half-life and tumor uptake was reported earlier by us and other laboratories (*14,19*). As the radioligand remains in the blood pool longer, the molecule has more time to accumulate at the target site.

M5A demonstrated high specificity toward the CEA, which was validated with in vivo experiments with directly labeled M5A ([^{89}Zr]Zr-DFO-M5A) and pretargeted **2** in CEA-positive (BxPC3) and CEA-negative (MIAPaCa-2) tumor–bearing mice (Fig. 4). Both imaging experiments in the 2 tumor models showed that the high specificity and excellent tumor-to-background signal that antibody-based imaging provides is not lost when the antibody imaging is done with the CB7-Adma pretargeting strategy. The obtained tumor-to-blood ratio of pretargeted **2** at 24 h after injection with the longer lag time schedule of 144 h was higher than that of [^{89}Zr]Zr-DFO-M5A at 72 h after injection (16.7 ± 4.6 and

7.5 ± 1.1, respectively) (Supplemental Tables 8 and 9). Interestingly, the fact that we were able to obtain excellent tumor targeting with a 144-h lag time suggests that even longer lag times may still be possible, which would further improve the dosimetry by reducing exposure in nontarget tissues, including blood and marrow. This would potentially improve image contrast using our pretargeted approach, as well as the therapeutic index when turning this strategy to targeted radionuclide therapy.

Previously, our laboratory reported the use of ferrocene radioligand–driven host–guest chemistry methodology for pretargeted PET (*13,14*). Comparing the CB7-ferrocene pair with the CB7-Adma pair as the pretargeting agents, we can note several advantages in the latter approach. All the investigated Adma radioligands maintained high in vitro stability in plasma up to 24 h, unlike the reported ferrocene radioligands (70%–80% intact at 4 h). Additionally, the formed Adma-CB7 host–guest complex exhibited higher in vivo stability than the previously reported CB7-ferrocene complex. We observed increasing tumor uptake in pretargeting experiments with **1**–**3** from the first studied time point (4 h) to the last (24 h), whereas the opposite trend was observed in the CB7-ferrocene pretargeting approach, and dissociation of the ferrocene radioligand from the CB7 over time is observed. All in all, when the same antibody, pretargeting schedule, dosing, and mouse tumor model were used, the highest tumor uptake values experienced with our lead Adma radioligand candidate (**2**) were several times higher (8 h, 5.9 ± 1.6 %ID/g; 24 h, 12.0 ± 0.9 ID/g) than for the previously reported ferrocene radioligand (8 h, 3.1 ± 0.6 %ID/g; 24 h, 1.5 ± 0.5 %ID/g) (*14*). The in vivo stability of a preformed CB7-Adma complex has been explored earlier with ^{11}C- and ^{18}F-labeled Adma guests in rodents (*9*). The complexes exhibited high stability in vivo; however, the stability was studied up to only 1 h. Our work expands knowledge on the in vivo formed host–guest complexes and their stability.

We hypothesize that a major advantage of host–guest pretargeting lies in the high stability of the CB7-Adma components, allowing pretargeting with flexible pretargeting dosing schedules and preferably longer lag times (>3 d). The reported pretargeting strategy excels with varying lag times, making the strategy clinically approachable. Importantly, the feasibility of longer lag times potentially allows the methodology to further decrease the whole-body radiation dose and increase the tumor-to-background signal—a motivation for shifting to pretargeting technologies from the use of directly radiolabeled antibodies.

CONCLUSION

We have reported the development and characterization of 3 Adma radioligands for CB7-Adma host–guest pretargeted PET. The use of a ^{64}Cu-labeled Adma radioligand along with a CB7-modified anti-CEA full-length antibody as the pretargeting agent pair for pretargeted PET in BxPC3 tumor–bearing nude mice resulted in high, enduring target uptake of the radioligand. To our knowledge, this is the first reported pretargeting study using CB7-Adma complex formation as the pretargeting interaction for antibody-based PET.

DISCLOSURE

KEY POINTS

QUESTION: Can host–guest complexation between a cucurbit[7]uril and an adamantane be used for pretargeting?

PERTINENT FINDINGS: A cucurbit[7]uril-modified antibody and a ^{64}Cu-labeled adamantane were administered separately intravenously to a mouse, and the biodistribution findings revealed that ^{64}Cu-labeled Adma specifically bound to the CB7-modified antibody.

IMPLICATIONS FOR PATIENT CARE: Clinical studies of pretargeting technologies have been hindered by the immunogenicity and lack of modularity of the pretargeting agents. The reported work reveals a promising new strategy for pretargeted nuclear medicine.

REFERENCES

1. Altai M, Membreno R, Cook B, Tolmachev V, Zeglis BM. Pretargeted imaging and therapy. *J Nucl Med.* 2017;58:1553–1559.
2. Jallinoja VI, Houghton JL. Current landscape in clinical pretargeted radioimmunoimaging and therapy. *J Nucl Med.* 2021;62:1200–1206.
3. Assaf KI, Nau WM. Cucurbiturils: from synthesis to high-affinity binding and catalysis. *Chem Soc Rev.* 2015;44:394–418.
4. Wanka L, Iqbal K, Schreiner PR. The lipophilic bullet hits the targets: medicinal chemistry of adamantane derivatives. *Chem Rev.* 2013;113:3516–3604.
5. Shetty D, Khedkar JK, Park KM, Kim K. Can we beat the biotin-avidin pair?: cucurbit[7]uril-based ultrahigh affinity host-guest complexes and their applications. *Chem Soc Rev.* 2015;44:8747–8761.
6. Zhao XB, Kang JY, Shi YP. Noncovalent dual-locked near-infrared fluorescent probe for precise imaging of tumor via hypoxia/glutathione activation. *Anal Chem.* 2022;94:6574–6581.
7. Sembo-Backonly BS, Estour F, Gouhier G. Cyclodextrins: promising scaffolds for MRI contrast agents. *RSC Advances.* 2021;11:29762–29785.
8. Wu H, Chen Z, Qi S, et al. Evaluation of the stability of cucurbit[8]uril-based ternary host-guest complexation in physiological environment and the fabrication of a supramolecular theranostic nanomedicine. *J Nanobiotechnology.* 2021;19:330.
9. Strebl MG, Yang J, Isaacs L, Hooker JM. Adamantane/cucurbituril: a potential pretargeted imaging strategy in immuno-PET. *Mol Imaging.* 2018;17:1536012118799838.
10. Girgis MD, Olafse T, Kenanova V, McCabe KE, Wu AM, Tomlinson JS. Targeting CEA in pancreas cancer xenografts with a mutated scFv-Fc antibody fragment. *EJNMMI Res.* 2011;1:24.
11. Yunis AA, Arimura GK, Russin DJ. Human pancreatic carcinoma (MIA PaCa-2) in continuous culture: sensitivity to asparaginase. *Int J Cancer.* 1977;19:128–135.
12. Tan MH, Nowak NJ, Loor R, et al. Characterization of a new primary human pancreatic tumor line. *Cancer Invest.* 1986;4:15–23.
13. Jallinoja VIJ, Carney BD, Zhu M, Bhatt K, Yazaki PJ, Houghton JL. Cucurbituril-ferrocene: host-guest based pretargeted positron emission tomography in a xenograft model. *Bioconjug Chem.* 2021;32:1554–1558.
14. Jallinoja VIJ, Carney BD, Bhatt K, et al. Investigation of copper-64-based host-guest chemistry pretargeted positron emission tomography. *Mol Pharm.* 2022;19:2268–2278.
15. Lindmo T, Bunn PA Jr. Determination of the true immunoreactive fraction of monoclonal antibodies after radiolabeling. *Methods Enzymol.* 1986;121:678–691.
16. Stabin MG, Sparks RB, Crowe E. OLINDA/EXM: the second-generation personal computer software for internal dose assessment in nuclear medicine. *J Nucl Med.* 2005;46:1023–1027.
17. Ulaner GA, Hyman DM, Lyashchenko SK, Lewis JS, Carrasquillo JA. ^{89}Zr-trastuzumab PET/CT for detection of human epidermal growth factor receptor 2–positive metastases in patients with human epidermal growth factor receptor 2–negative primary breast cancer. *Clin Nucl Med.* 2017;42:912–917.
18. Menke-van der Houven van Oordt CW, Gootjes EC, Huisman MC, et al. ^{89}Zr-cetuximab PET imaging in patients with advanced colorectal cancer. *Oncotarget.* 2015;6:30384–30393.
19. Meyer JP, Kozlowski P, Jackson J, et al. Exploring structural parameters for pretargeting radioligand optimization. *J Med Chem.* 2017;60:8201–8217.
20. Obach RS, Lombardo F, Waters NJ. Trend analysis of a database of intravenous pharmacokinetic parameters in humans for 670 drug compounds. *Drug Metab Dispos.* 2008;36:1385–1405.
21. Lewis JS, Windhorst AD, Zeglis BM. *Radiopharmaceutical Chemistry.* Springer Cham; 2019;125–127.